

A master equation for a spatial population model with pair interactions

Daniel A. Birch*, William R. Young

Scripps Institution of Oceanography, University of California at San Diego, La Jolla, CA 92093-0213, USA

Received 9 February 2005

Available online 25 January 2006

Abstract

We derive a closed master equation for an individual-based population model in continuous space and time. The model and master equation include Brownian motion, reproduction via binary fission, and an interaction-dependent death rate moderated by a competition kernel. Using simulations we compare this individual-based model with the simplest approximation, the spatial logistic equation. In the limit of strong diffusion the spatial logistic equation is a good approximation to the model. However, in the limit of weak diffusion the spatial logistic equation is inaccurate because of spontaneous clustering driven by reproduction. The weak-diffusion limit can be partially analyzed using an exact solution of the master equation applicable to a competition kernel with infinite range. This analysis shows that in the case of a top-hat kernel, reducing the diffusion can increase the total population. For a Gaussian kernel, reduced diffusion invariably reduces the total population. These theoretical results are confirmed by simulation.

© 2006 Elsevier Inc. All rights reserved.

Keywords: Clustering; Competition kernel; Diffusion–reaction; Individual-based model; Logistic equation; Master equation; Pattern formation; Population dynamics; Reproductive pair correlations; Spatial dynamics

1. Introduction

Pioneering works in population biology proposed the spatial logistic equation (SLE),

$$C_t = \gamma C - \eta C^2 + \kappa \nabla^2 C, \quad (1)$$

as a model for the growth (γ), saturation (η), and dispersal (κ) of a population or gene (Fisher, 1937; Kolmogorov et al., 1937; Skellam, 1951). Here $C(x, t)$ is the “concentration” of a species, defined via a sample region dx surrounding a point x at time t as

$$C(x, t) dx = \text{expected number of organisms in } dx. \quad (2)$$

Our goal here is to better understand how (1) approximates an individual-based model. The analogous problem in physics is the derivation of advection–diffusion–reaction (ADR) equations starting from a many-body formulation. A key issue in passage from an individual-based model to an ADR description, such as (1), is local fluctuations in population density arising from the discrete nature of

individuals and the randomness of birth and death. Emphasizing the importance of birth and death at an individual level, Bolker and Pacala (1997) refer to these fluctuations as “demographic stochasticity.” In statistical physics similar fluctuations arising from the atomistic structure of matter are known as “intrinsic noise” (van Kampen, 1997).

1.1. The Brownian bug model

The individual-based model studied here is an assembly of organisms (“bugs”) moving through continuous space and time via diffusion (with diffusivity κ). The bugs reproduce by binary fission at a constant rate, λ , and die at the rate determined by an intrinsic constant death rate, μ , plus an extra density-dependent contribution.

To simplify the model we make the assumption that the density dependence of the death rate arises only from interactions between *pairs* of organisms. The interaction between two individuals separated by a distance r is quantified by a “competition” kernel, $v(r)$ (Bolker and Pacala, 1997; Dieckmann et al., 2000—BDLMP hereafter). The mathematical statement of this assumption is that in a

*Corresponding author.

E-mail addresses: dbirch@ucsd.edu (D.A. Birch), wryoung@ucsd.edu (W.R. Young).

population with k bugs, the death rate of bug q , located at \mathbf{x}_q , is

$$\text{death rate of bug } q = \mu + \sum_{\substack{p=1 \\ p \neq q}}^k v(|\mathbf{x}_p - \mathbf{x}_q|). \quad (3)$$

Above, μ is the constant intrinsic death rate. The second term on the right-hand side of (3) is the interaction of bug q with the other $k - 1$ bugs in the population. The competition kernel, $v(r)$, is a positive function so that interaction between bugs increases the probability of death.

The competition kernel does not have to be interpreted literally as competition for a limited resource, nor is it the only means of modeling such an interaction. For example, Hernández-García and López (2004, 2005) use a density-dependent birth rate. In the ecological literature, Bolker and Pacala (1999) employ a similar strategy using an “establishment probability” to model competition in plant populations. Other possible interpretations of (3) include cannibalism or the attraction of predators to clusters of prey. Martin (2004) models nutrient limitation using a hybrid model with individual organisms in continuous space consuming nutrients defined on a lattice.

The models of Bolker and Pacala (1997, 1999) and Law et al. (2003) are directed at perennial plant populations. In this context, dispersal is coupled to birth by using a “dispersal kernel” to give each new plant a random displacement from its parent. On the other hand, Brownian bugs move incessantly as random walkers. See Appendix A for a description of the implementation of the Brownian bug model.

Young et al. (2001) originally used the term “Brownian bug” for the special case $v(r) = 0$. Here we use “Brownian bugs” to refer to the individuals in the more general model described above.

1.2. The Poisson assumption

We have now introduced two models—the spatial logistic equation in (1) and the individual-based Brownian bug model. The first is an approximation to the second if the *Poisson assumption* is valid. The analog in statistical physics is the assumption of molecular chaos. The Poisson assumption enters the derivation of the ADR equation (1) through the pair function, $G(\mathbf{x}, \mathbf{y}, t)$, defined by¹

$$\begin{aligned} G(\mathbf{x}, \mathbf{y}, t) \, d\mathbf{x} \, d\mathbf{y} \\ = \text{expected number of pairs of organisms with} \\ \text{one member in } d\mathbf{x} \text{ and the other in } d\mathbf{y}. \end{aligned} \quad (4)$$

C and G are the first two members of a hierarchy of “spatial moments” or “reduced distribution functions.”

¹We do not count each individual as a pair with itself, but we do count the pair 1 and 2 as distinct from 2 and 1. Thus in a domain containing n singletons, there are $n(n - 1)$ pairs. The integral of $C(\mathbf{x})$ over \mathbf{x} is the expected value of n , and the integral of $G(\mathbf{x}, \mathbf{y})$ over \mathbf{x} and \mathbf{y} is the expected value of $n^2 - n$.

Higher members of the hierarchy, such as the triplet function, $T(\mathbf{x}, \mathbf{y}, \mathbf{z}, t)$, describe correlations between the positions of three or more organisms. For independently distributed (uncorrelated) points the higher spatial moments factor into products of the concentration: $G(\mathbf{x}, \mathbf{y}, t) = C(\mathbf{x}, t)C(\mathbf{y}, t)$, $T(\mathbf{x}, \mathbf{y}, \mathbf{z}, t) = C(\mathbf{x}, t)C(\mathbf{y}, t)C(\mathbf{z}, t)$, etc.

A systematic derivation of the continuum equations corresponding to the Brownian bug model results in

$$C_t = \gamma C - \int v(|\mathbf{x} - \mathbf{y}|)G(\mathbf{x}, \mathbf{y}, t) \, d\mathbf{y} + \kappa \nabla^2 C, \quad (5)$$

where $\gamma \equiv \lambda - \mu$ is the net intrinsic growth rate (see BDLMP and Section 5). Eq. (5) is exact: the convolution term is the expected death rate of a bug at \mathbf{x} due to interaction with neighboring bugs. In the context of diffusively limited chemical reactions the competition kernel $v(r)$ is known as the reaction kernel, and (5) has long been appreciated as a fundamental connection between the concentration, C , and the pair function, G (e.g., Doi, 1976a, b).

To obtain the spatial logistic equation (1) from the exact expression (5) one first makes the Poisson approximation

$$G(\mathbf{x}, \mathbf{y}, t) \approx C(\mathbf{x}, t)C(\mathbf{y}, t), \quad (6)$$

and pulls $C(\mathbf{x}, t)$ outside the \mathbf{y} -integral in (5). Then, with a further scale separation assumption, one has

$$C(\mathbf{x}, t) \int v(\mathbf{x} - \mathbf{y})C(\mathbf{y}, t) \, d\mathbf{y} \approx \eta C^2(\mathbf{x}, t), \quad (7)$$

where

$$\eta \equiv \int v(|\mathbf{y}|) \, d\mathbf{y}. \quad (8)$$

While the validity of these ad hoc approximations is not obvious, the intuitive content of (6) is that there are no correlations between the positions of individuals. Roughly speaking, one trusts that this assumption is justified if diffusion is strong enough. The upshot is that density-dependent population controls, involving *pairs* of organisms, are approximated in terms of the singleton descriptor, $C(\mathbf{x}, t)$; this is the origin of the term ηC^2 in (1). Note that the density dependence does not have to come from the mortality term: a density-dependent birth rate results in the same SLE.

For recent work on a nonlocal version of the SLE equation (1), obtained by using approximation (6), but not approximation (7), see Fuentes et al. (2004), Shnerb (2004), Hernández-García and López (2004, 2005), and Maruvka and Shnerb (2005).

1.3. Reproductive pair correlations

The reproduction of discrete individuals is a compelling reason to expect important non-Poisson fluctuations and the failure of (6). Brownian bugs (and any real organisms which reproduce via binary fission) are born next to their

siblings. Therefore, reproduction ineluctably creates non-Poisson spatial correlations between pairs (daughter cells) of individuals and these correlations are neglected by the approximation (6) and the ADR approach.

The development of reproductive pair correlations is illustrated in Fig. 1 using an example studied by Felsenstein in 1975. Felsenstein's problem is the special case of the Brownian bug model with $v(r) = 0$ and $\gamma \equiv \lambda - \mu = 0$; the average population is constant because the intrinsic birth rate λ is equal to the death rate μ . With these simplifications there are no interactions between the bugs: birth and death are independent of the spatial distribution of the population. Yet the system is still nontrivial. Felsenstein (1975) showed that the patches in Fig. 1 grow larger and farther apart with increasing time (see also Young et al., 2001). Mathematicians refer to this special case $v(r) = 0$ of the Brownian bug model as “super-Brownian motion” (Adler, 1997; Etheridge, 2000; Slade, 2002). The unrestrained clumping produced with $v(r) = 0$ has been independently studied by statistical physicists (Zhang et al., 1990; Meyer et al., 1996; Kessler et al., 1997).

With $\gamma \equiv \lambda - \mu = 0$ and $v(r) = \eta = 0$, both (1) and (5) collapse to the diffusion equation

$$C_t = \kappa \nabla^2 C. \quad (9)$$

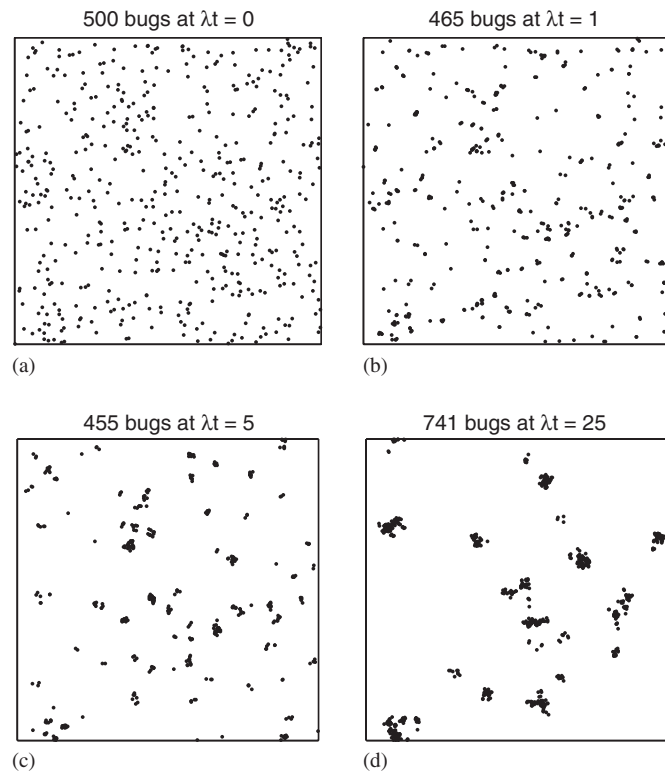


Fig. 1. Clustering due to reproductive pair correlations in the Brownian bug model. The simulation above uses the Monte Carlo method described in Appendix A with $\lambda = \mu = 1$, $v(r) = 0$ and $\kappa = 10^{-5}$. The domain is the unit square ($L = 1$ and $d = 2$) with reentrant boundary conditions. The total population changes due to random differences between the number of births and deaths.

If there are initially N bugs in the doubly periodic $L \times L$ domain then the solution of (9) with the initial condition $C(\mathbf{x}, 0) = N/L^2$ is $C(\mathbf{x}, t) = N/L^2$. This answer is correct: the solution of the diffusion equation (9) is the *ensemble average* of many realizations of Fig. 1. However, because of reproductive pair correlations the *typical realization* in Fig. 1 is dominated by demographic stochasticity and is very different from the ensemble average. In other words, fluctuations are so large that $C(\mathbf{x}, t)$ by itself is an insufficient characterization of the process. Instead the pair function, $G(\mathbf{x}, t)$ in (4), carries information about the size and spacing of the clumps (see Section 3).

1.4. The plan

In this article we provide an exact deterministic formulation of the Brownian bug model using an approach known in statistical physics as the master equation. The master equation contains complete and detailed information concerning all of the statistical properties of the Brownian bug model. In a related problem, Bolker and Pacala (1997) and Law et al. (2003) (BDLMP) have developed an alternative approach, based on an unclosed hierarchy of spatial moments. We show that the BDLMP hierarchy is obtained as a reduction of the master equation. The master equation is also very complicated and is unlikely to permanently replace either ADR or the BDLMP hierarchy in our affections. Nonetheless, it is useful to possess an exact formulation without closure assumptions: one can hope to eventually justify the moment closure strategy by identifying a non-dimensional parameter permitting asymptotic reduction of the master equation.

Section 2 is devoted to direct numerical simulation of the Brownian bug model. The goal is to survey the parameter space and illustrate the success of (1) in the strong-diffusion limit, and its failure when diffusion is weak. A surprising result of Section 2 is that depending on the details and strength of the competition kernel the population may increase or decrease in the weak-diffusion limit. In Sections 3 and 4 we formulate a stochastic population model in continuous space without resort to the BDLMP hierarchy. The resulting master equation is (44). In Section 5 we show that the BDLMP hierarchy follows from this master equation. In Section 6 we obtain an exact solution of the master equation of Section 4 by considering the unrealistic case of a competition kernel with infinite range. In Section 7 we use the exact solution from Section 6 to explain the result from Section 2 that population can increase in response to decreased dispersal. Section 7 also discusses the dependence of our results on the structure of the competition kernel. Section 8 is the conclusion.

2. Simulations and overview of the Brownian bug model

When $v(r) = 0$ (as in Fig. 1), the only ingredient in the Brownian bug model with any pretense to biological reality

is that a reproductive event introduces the new individuals at the same location as the parent. The patches evident in Fig. 1 are produced solely by this mechanism and do not require any other interactions between bugs. Felsenstein (1975) noted that with $v(r) = 0$, the model flagrantly violates reality because of the absence of density-dependent population regulation. The problem is more realistic when a density limiting interaction is included, such as $v(r) \neq 0$ (Bolker and Pacala, 1997; Law et al., 2003). Our goal in this section is to illustrate the behavior of the Brownian bug model in this case using numerical simulation. Consider then the case of pairwise competition, $v(r) \neq 0$ in (3). A simple example of local interaction is the “top-hat” competition kernel, defined by

$$v(r) = \begin{cases} v_0 & \text{if } r < a, \\ 0 & \text{if } r \leq a. \end{cases} \quad (10)$$

With the model above, η in (8) is equal to $v_0 \pi a^2$.

We are interested in the case where the length scale of the spatial domain (e.g., L for an $L \times L$ square) is much larger than the range of the competition kernel, a . In other words, a/L is the first non-dimensional parameter and we are concerned with the regime

$$\frac{a}{L} \ll 1. \quad (11)$$

Using the birth rate, λ , to define a time scale, there are two other non-dimensional parameters: μ/λ and v_0/λ . The fourth non-dimensional parameter,

$$a_* \equiv a \sqrt{\frac{\lambda}{\kappa}}, \quad (12)$$

is a measure of the strength of diffusion. The four non-dimensional parameters above completely specify the Brownian bug model with the top-hat competition kernel (10).

2.1. Simulations using the top-hat kernel and $\mu = 0$

Fig. 2 shows the total population as a function of time for four different values of the parameter a_* . The dashed line shows the population predicted by the SLE. The SLE prediction is the equilibrium solution (or carrying capacity) of (1), $C = \gamma/\eta$, times the area L^2 :

$$N_0 \equiv \frac{L^2(\lambda - \mu)}{\pi a^2 v_0}. \quad (13)$$

(Recall that $\gamma \equiv \lambda - \mu$ is the net intrinsic growth rate.) In the case with strong diffusion ($a_* = 1$ in Fig. 2) the population fluctuates around N_0 ; at $a_* = 4$ the SLE prediction is a little too high. However, for weak diffusion ($a_* = 16$ and 64) the population is distinctly greater than N_0 . Thus under the top-hat kernel the average population depends non-monotonically on the diffusivity (equivalently a_*).

Snapshots of the final states of the simulations in Fig. 2 are shown in Fig. 3. Panel (a) shows the example with

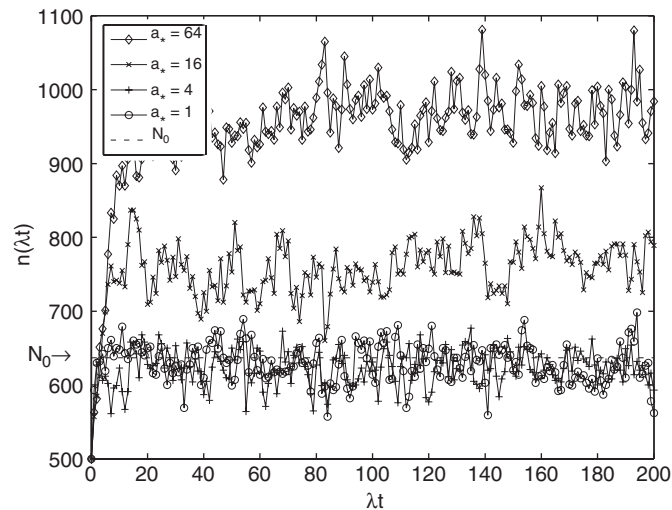


Fig. 2. The population as a function of time for four simulations of the Brownian bug model with density-dependent death rate using the top-hat kernel. The parameters are $a/L = \frac{1}{10}$, $\lambda/v_0 = 20$, $\mu = 0$, and $a_* \equiv a\sqrt{\lambda/\kappa}$ as noted in the legend. The dashed line is the SLE prediction, N_0 , in (13).

strong diffusion, $a_* = 1$; in this case the spatial statistics are close to Poisson (see Section 3 for a quantitative assessment using the pair function). For weak diffusion, that is, large a_* , the population shows strong clustering—each isolated cluster in panels (c) and (d) of Fig. 3 is a family descended from a single individual. These clusters in panels (c) and (d) indicate the failure of the Poisson assumption (6).

Given the strong clustering with $a_* = 16$ and 64 , it is not unexpected that the SLE prediction (13) is inaccurate. The surprise in Figs. 2 and 3 is that with weak diffusion ($a_* = 16$ and 64) the population is elevated well above N_0 in (13). This is nonintuitive: one expects a reduction in net death rate (and hence a higher equilibrium density) the greater the capacity of bugs to escape from competition with their relatives. In Fig. 3(c) and (d), weakly diffusing bugs huddle together in dense, isolated family clusters, but nonetheless, the total equilibrium population in Fig. 3(c) and (d) is higher than that of the strongly diffusing case in Fig. 3(a). The key to understanding this curious property of the weak-diffusion limit is that the increased familial competition is compensated by even more strongly decreased competition with unrelated bugs (see Section 7). We now show that with the top-hat kernel this peculiar inverse relation between diffusion and population is found in a large portion of the parameter space.

Fig. 4 shows a survey of the average population, N , as a function of a_* and λ/v_0 (with $\mu/\lambda = 0$ and $L/a = 10$). The results in Fig. 4 are obtained by estimating the average population from 240 simulations, similar to the 4 shown in Fig. 2. To obtain stable estimates of the average population we averaged over long times. For all values of λ/v_0 in Fig. 4 the population tends towards N_0 in the strong-diffusion limit ($a_* \rightarrow 0$). This is consistent with the intuition that strong diffusion enables a bug to quickly explore a large environment and so to “feel” the average concentration.

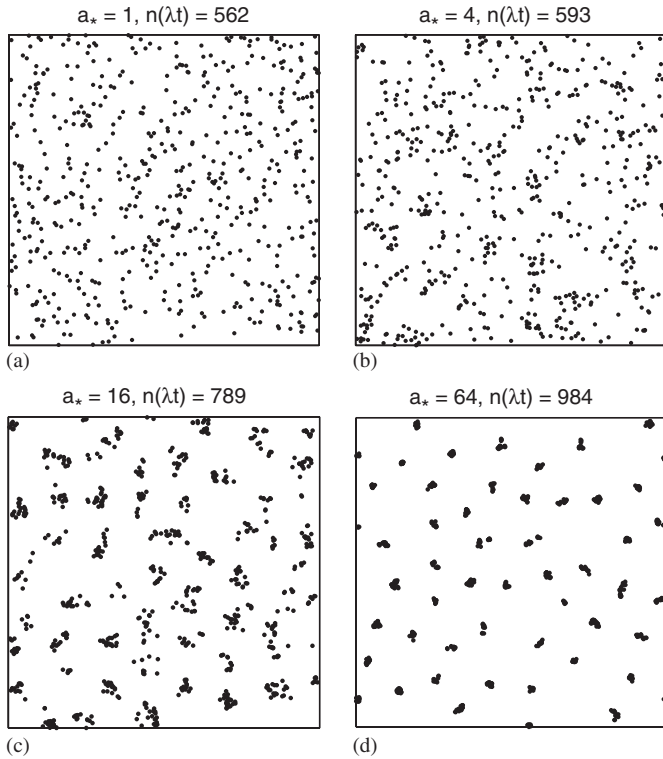


Fig. 3. Snapshots of Brownian bugs in equilibrium (the ending states of the simulations in Fig. 2). Notice that the system with weak diffusion (large a_*) is both clustered and has a larger population than the strong diffusion case in panel (a). The parameters of these four simulations are $\lambda t = 200$, $a/L = \frac{1}{10}$, $\lambda/v_0 = 20$, $\mu = 0$, and a_* as indicated in the titles. n is the instantaneous population.

Alternatively, strong diffusion wipes out the non-Poisson correlations generated by reproduction and establishes the Poisson independence condition (6). The result also indicates that in the strong-diffusion limit the only relevant property of the competition kernel is the integral η in (8).

In Fig. 4 all the curves fall below $N/N_0 = 1$ if a_* is sufficiently small. But once a_* is greater than about 5 the situation is more complicated: N/N_0 then has a strong dependence on both a_* and λ/v_0 . It seems unlikely that there is any simple and comprehensive characterization of the dependence of N/N_0 on a_* and λ/v_0 .

2.2. The Gaussian competition kernel

The curves with $\lambda/v_0 = 20$ and 40 in Fig. 4 agree with the results obtained by Hernández-García and López (2004). These authors, also using a top-hat kernel, showed that the population of bugs with a density-dependent birth rate decreased with increased advection.

The results in Fig. 4 disagree with those of Bolker and Pacala (1997) and Law et al. (2003). Both of these groups found that increasing dispersal increases the equilibrium population in their individual-based models and can increase the population above the mean-field prediction. We were unpleasantly surprised to discover that this

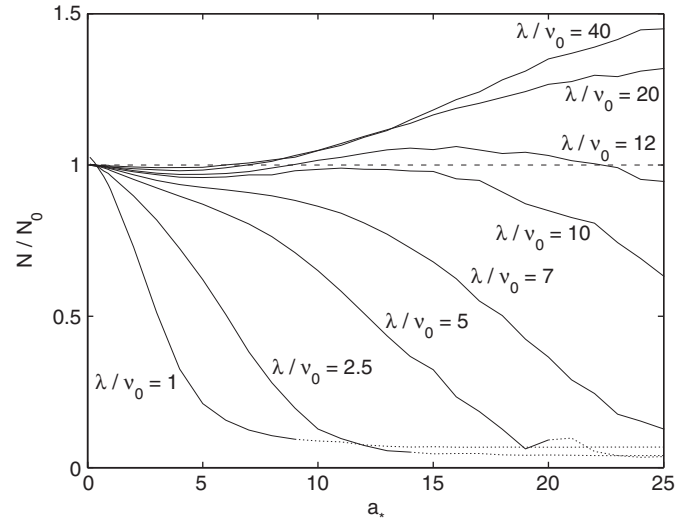


Fig. 4. The average population divided by the SLE prediction (13) as a function of $a_* \equiv a\sqrt{\lambda/\kappa}$. This figure summarizes the results of 240 simulations using the top-hat kernel in (10). The SLE prediction fails for large a_* (weak diffusion). The other parameters are $a/L = \frac{1}{10}$ and $\mu = 0$; because $\mu = 0$ extinction is impossible. The dotted lines indicate the non-percolating regimes.

discrepancy is due to the form of the competition kernel. Specifically, Fig. 4 is based on the compact top-hat kernel (10), while Bolker and Pacala (1997) use a Laplacian kernel and Law et al. (2003) employ a Gaussian kernel:

$$v(r) = \frac{\eta}{2\pi\ell^2} e^{-r^2/2\ell^2}. \quad (14)$$

Repeating our simulations with the Gaussian kernel (14) we find that the average population always decreases monotonically with decreasing dispersal (see Fig. 5). However, we do not find that increasing dispersal increases the population above N_0 ; this difference may be due to Bolker and Pacala (1997) and Law et al. (2003) using models with instantaneous long-range dispersal and our using a model with binary fission and diffusion. Section 7 has further discussion of the differences between the Gaussian and top-hat kernels.

2.3. Nonzero intrinsic death rate, $\mu \neq 0$

Our earlier discussion of the top-hat kernel considered only the special case $\mu = 0$ (i.e., the intrinsic death rate is zero in the simulations used to generate Figs. 2–5). In Fig. 6 we consider $\mu \neq 0$ and verify that the counterintuitive increase of the population with decreasing diffusion persists with nonzero intrinsic mortality.

With nonzero μ eventual extinction due to a large fluctuation is guaranteed.² However, the extinction time becomes exponentially long as the system size increases and so in practice one observes a quasi-stationary state in which

²Extinction is impossible if $\mu = 0$ since a state with one bug can never transition to zero bugs.

the population fluctuates about some mean level (e.g., Doering et al., 2005). The typical population fluctuations in these $\mu \neq 0$ quasi-equilibria are qualitatively similar to those in Fig. 2 with $\mu = 0$. Thus in the simulations with nonzero μ we report the “quasi-equilibrium” population, N , and

compare N to the SLE prediction N_0 in (13). This is illustrated in Fig. 6(a), which shows the population as a function of time. The initial population is 500 in all cases and one can see that the bugs rapidly adjust to their (quasi-) equilibrium populations for $\mu/\lambda = 0.0$ and 0.2. With $\mu/\lambda = 0.4$ the population becomes extinct.

Fig. 6(b) shows the quasi-equilibrium population as a function of μ/λ with fixed λ/v_0 and a_* . This shows that the increase in population above N_0 with weak diffusion and the top-hat kernel is a robust effect which persists for μ/λ up to about 0.2. For $\mu/\lambda > 0.35$ fluctuations result in rapid extinction and no quasi-equilibrium population is obtained.

2.4. The percolation transition with $\mu = 0$

The percolation transition, illustrated in Figs. 7 and 8, is a watershed in the $(a_*, \lambda/v_0)$ parameter space. If a_* is small and λ/v_0 is large then a single initial bug will eventually populate the domain with its descendants. This is the percolating regime: the expanding family of an ur-bug invades, and eventually fills, an initially empty domain. On the other hand, if a_* is large and λ/v_0 is small then a single bug cannot start an expanding family: pair interactions kill the bugs before they manage to escape from each other’s competition circles. (In this subsection we return to the case $\mu = 0$, so that extinction is impossible.) A non-percolating species is maladapted, and the non-percolating regime has little biological relevance. Nonetheless, for a complete characterization of the Brownian bug model, it is important to appreciate the distinction between the percolating and

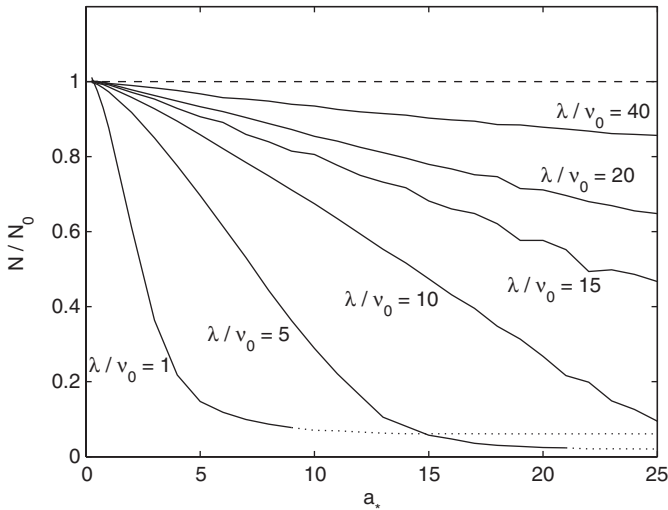


Fig. 5. The average population divided by the SLE prediction (13) as a function of $a_* \equiv 2\ell\sqrt{\lambda/\kappa}$. The simulations above employ the Gaussian competition kernel in (14). In contrast to Fig. 4 the total population decreases monotonically with diffusion. The definition $a_* \equiv 2\ell\sqrt{\lambda/\kappa}$ associates a length $a = 2\ell$ with the Gaussian kernel in (14). This ensures that the squared “radius of gyration”, $\int r^2 v(r) dr / \int v(r) dr$, is equal to $a^2/2$ for both the Gaussian and top-hat kernels. As in Fig. 4, $\mu = 0$ and $a/L = \frac{1}{10}$.

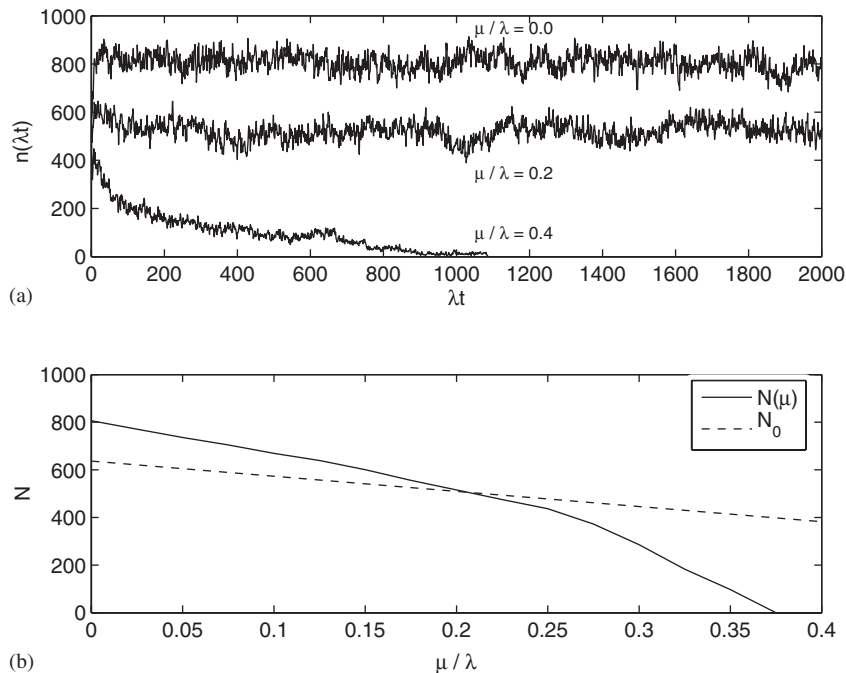


Fig. 6. (a) $n(\lambda t)$ for $\mu/\lambda = 0.0, 0.2, 0.4$. (b) The total population N compared to N_0 in (13); $\lambda/v_0 = 20$ and $a_* = 20$ in all cases. $N > N_0$ for all $\mu/\lambda < 0.2$, indicating that the enhanced population under weak diffusion and the top-hat kernel persists with $\mu \neq 0$.

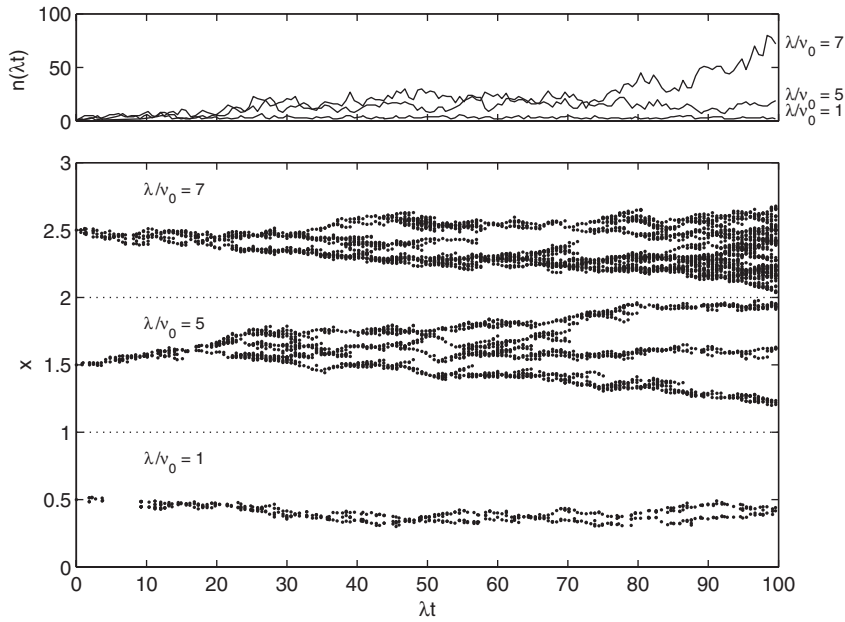


Fig. 7. Three simulations with $n(0) = 1$, $\mu = 0$, $a_* \equiv a\sqrt{\lambda/\kappa} = 10$ and the top-hat kernel. Only the x -coordinate of each bug is plotted. The $\lambda/v_0 = 5$ and 7 cases are offset by 1 and 2 for clarity. The bugs percolate for $\lambda/v_0 = 5$ and 7, but not for $\lambda/v_0 = 1$. The large gaps indicate time intervals during which no events occurred.

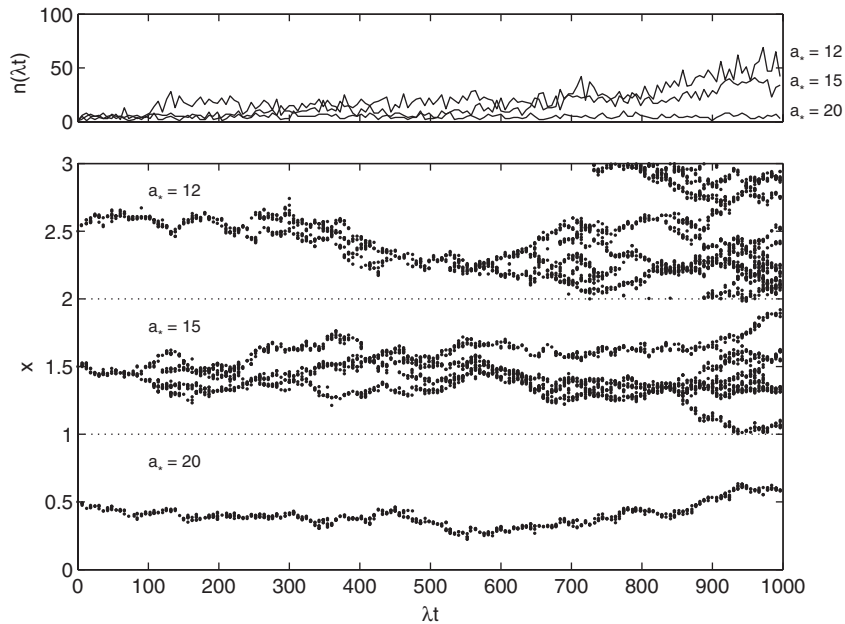


Fig. 8. Three simulations with $n(0) = 1$, $\mu = 0$, $\lambda/v_0 = 5$ and the top-hat kernel. Only the x -coordinate of each bug is plotted. The $a_* = 15$ and 12 cases are offset by 1 and 2 for clarity. The bugs percolate for $a_* = 15$ and 12, but not for $a_* = 20$.

non-percolating regimes. In Figs. 4 and 5 we indicate the non-percolating cases by dotting the curves.

Fig. 7 shows the populations and x -coordinates of the bugs in three runs, each beginning with a single bug. The upper plot shows the population as a function of time for each of three values of λ/v_0 : 1, 5, and 7. The value of a_* is 10 in all cases and all of the runs start with a single initial bug. The lower plot shows the x -coordinates of each bug.

The cases of $\lambda/v_0 = 5$ and 7 are percolating. Interestingly, the expanding population is strongly clustered even as it diffuses to fill the domain. The case of $\lambda/v_0 = 1$ is not percolating. Occasionally clusters of bugs will live long enough to diffuse away from each other. But eventually the clusters collide and one is eliminated.

Fig. 8 also shows two cases of percolation and one case of non-percolation. $\lambda/v_0 = 5$ in all cases and again the

simulations are started with a single initial bug. In the cases of $a_* = 12$ and 15 the bugs percolate. However, in the weakest diffusion case ($a_* = 20$) the bugs do not percolate. Note that Fig. 7 uses stronger diffusion ($a_* = 10$) than any of the cases in Fig. 8. Together Figs. 7 and 8 show that percolation depends on both the birth rate and the diffusivity.

3. Fock space formulation for population dynamics

The Fock space is a tool for studying the spatial patterns formed by stochastically evolving populations. We begin by summarizing the formalism; for more details, Chapter II of van Kampen (1997) is a useful reference. Suppose that a variable number of bugs are reproducing and dying in a d -dimensional space. For example, in a three-dimensional space ($d = 3$) bug p is at position $\mathbf{x}_p = (x_p, y_p, z_p)$. The total volume of the domain is denoted by Ω . The dimensions of Ω are (length) ^{d} .

At time t , the population is specified by the population size, k , and a vector, \mathbf{X}_k , containing the positions of all k bugs:

$$\mathbf{X}_k \equiv [\mathbf{x}_1, \mathbf{x}_2, \dots, \mathbf{x}_k]. \quad (15)$$

The Fock space is the set of all possible states. The probability distribution over the Fock space is given by a set of non-negative functions, $F_k(\mathbf{X}_k, t)$, defined such that

$$F_k(\mathbf{X}_k, t) d\mathbf{X}_k = \text{Pr} \{k \text{ bugs, with a bug in } d\mathbf{x}_1, \text{ another in } d\mathbf{x}_2 \text{ etc.}\}. \quad (16)$$

The normalization is

$$F_0(t) + \int F_1(\mathbf{X}_1, t) d\mathbf{X}_1 + \int F_2(\mathbf{X}_2, t) d\mathbf{X}_2 + \dots = 1. \quad (17)$$

Bugs are indistinguishable, so we can freely exchange \mathbf{x}_p and \mathbf{x}_q ; this is the permutation symmetry of F_k :

$$F_k(\mathbf{x}_1, \dots, \mathbf{x}_p, \dots, \mathbf{x}_q, \dots, \mathbf{x}_k, t) = F_k(\mathbf{x}_1, \dots, \mathbf{x}_q, \dots, \mathbf{x}_p, \dots, \mathbf{x}_k, t). \quad (18)$$

Any function A defined on the Fock space consists of

$$\{A_0, A_1(\mathbf{X}_1), A_2(\mathbf{X}_2), \dots\}. \quad (19)$$

The expectation of A is a sum over k as well as, for each k , a k -fold integral:

$$\langle A \rangle \equiv A_0 F_0(t) + \sum_{k=1}^{\infty} \int A_k(\mathbf{X}_k) F_k(\mathbf{X}_k, t) d\mathbf{X}_k. \quad (20)$$

If $A_k = 1$ then (20) collapses to the normalization condition in (17). Notice that an expectation may be time- and space-dependent, such as the expected density of bugs at a particular location in a temporally evolving and spatially inhomogeneous system.

3.1. Reduced distribution functions

Consider a sample volume \mathcal{V} and let $\chi(\mathbf{x})$ be the indicator function of \mathcal{V} . That is, $\chi(\mathbf{x}) = 1$ if $\mathbf{x} \in \mathcal{V}$ and $\chi(\mathbf{x}) = 0$ otherwise. Denote the number of bugs in \mathcal{V} by n . n is a random variable and using the definition of expectation in (20), with $A_k = \sum_{p=1}^k \chi(\mathbf{x}_p)$, we get

$$\begin{aligned} \langle n \rangle &= \left\langle \sum_{p=1}^k \chi(\mathbf{x}_p) \right\rangle \\ &= \sum_{k=1}^{\infty} \int \sum_{p=1}^k \chi(\mathbf{x}_p) F_k(\mathbf{X}_k) d\mathbf{X}_k. \end{aligned} \quad (21)$$

Using the permutation symmetry (18) the k terms in the sum over p are all equal to the term with $p = 1$. Thus,

$$\begin{aligned} \langle n \rangle &= \sum_{k=1}^{\infty} k \int \chi(\mathbf{x}_1) F_k(\mathbf{X}_k) d\mathbf{X}_k \\ &= \int \chi(\mathbf{x}_1) f^{(1)}(\mathbf{x}_1, t) d\mathbf{x}_1, \end{aligned} \quad (22)$$

where the *concentration* or density of bugs is

$$f^{(1)}(\mathbf{x}, t) \equiv \sum_{k=1}^{\infty} k \int F_k(\mathbf{x}, \mathbf{X}_{k-1}, t) d\mathbf{X}_{k-1}. \quad (23)$$

The concentration can be written more intuitively as

$$f^{(1)}(\mathbf{x}, t) = \left\langle \sum_{p=1}^k \delta(\mathbf{x} - \mathbf{x}_p) \right\rangle. \quad (24)$$

Eq. (24) may be verified by plugging into the definition of the expectation (20) and once again obtaining (23).

The function $f^{(1)}(\mathbf{x}, t)$ is exactly the same as the concentration, $C(\mathbf{x}, t)$, introduced previously in (2). In this section we prefer the notation $f^{(1)}$ to emphasize that the concentration is the first function in a hierarchy of *reduced distribution functions* or *spatial moments* (see BDLMP). One essential point is that $\langle \rangle$ denotes the average computed according to the definition in (20). Thus the concentration is defined via an ensemble average, $\langle \rangle$, rather than by coarse graining. A glance at Fig. 1 or 3 shows that this distinction is important.

Next, consider the expected value of n^2 :

$$\langle n^2 \rangle = \left\langle \sum_{p=1}^k \sum_{q=1}^k \chi(\mathbf{x}_p) \chi(\mathbf{x}_q) \right\rangle. \quad (25)$$

Using the definition of $\langle \rangle$ in (20) and the permutation symmetry (18) we find that

$$\langle n^2 - n \rangle = \int \int f^{(2)}(\mathbf{x}, \mathbf{y}, t) \chi(\mathbf{x}) \chi(\mathbf{y}) d\mathbf{x} d\mathbf{y}, \quad (26)$$

where

$$f^{(2)}(\mathbf{x}, \mathbf{y}, t) = \sum_{k=2}^{\infty} k(k-1) \int F_k(\mathbf{x}, \mathbf{y}, \mathbf{X}_{k-2}, t) d\mathbf{X}_{k-2} \quad (27)$$

$$= \left\langle \sum_{\substack{p,q=1 \\ p \neq q}}^k \delta(\mathbf{x} - \mathbf{x}_p) \delta(\mathbf{y} - \mathbf{x}_q) \right\rangle. \quad (28)$$

The function $f^{(2)}$ is the same as the pair function, G , defined in (4). Two other interpretations are helpful. First, the ratio $f^{(2)}(\mathbf{x}, \mathbf{y})/f^{(1)}(\mathbf{x})f^{(1)}(\mathbf{y})$ is the probability of having bugs at \mathbf{x} and \mathbf{y} relative to the probability of having bugs at \mathbf{x} and \mathbf{y} if the bugs were independently distributed. Second, the ratio $f^{(2)}(\mathbf{x}, \mathbf{y}) d\mathbf{y}/f^{(1)}(\mathbf{x})$ is the conditional probability of having an individual at $d\mathbf{y}$, given that there is an individual at \mathbf{x} .

The functions $f^{(1)}(\mathbf{x}, t)$ and $f^{(2)}(\mathbf{x}, \mathbf{y}, t)$ are the beginning of an infinite hierarchy of reduced distribution functions. The reduced distribution function of order s , $f^{(s)}(\mathbf{x}_1, \mathbf{x}_2, \dots, \mathbf{x}_s, t)$, is

$$f^{(s)}(\mathbf{X}_s, t) \equiv \sum_{k=s}^{\infty} \frac{k!}{(k-s)!} \int F_k(\mathbf{X}_s, \mathbf{X}_{k-s}, t) d\mathbf{X}_{k-s}. \quad (29)$$

3.2. Some examples of the pair function $f^{(2)}$

As an illustrative example of the descriptors $f^{(1)}$ and $f^{(2)}$, consider the four simulations shown in Fig. 3. Because the system is spatially homogeneous, the concentration $f^{(1)}$ (defined via an ensemble average) is constant in each of the four cases. Thus the concentration does not usefully distinguish between the different cases in Fig. 3.

On the other hand, the pair descriptor $f^{(2)}$ gauges the size and spacing of the patches in Fig. 3. Fig. 9 shows estimates of the radial distribution function, $g(r)$, defined by $g(r) \equiv f^{(2)}(r)/f^{(1)2}$. This definition of $g(r)$ is motivated by considering that $g(r) = 1$ (actually $1 - 1/n$, but we are interested in large n) for a Poisson process. An intuitive interpretation of the radial distribution function is provided by

$$f^{(1)}g(r) = \text{average density of bugs at a distance } r \text{ from a tagged bug.} \quad (30)$$

The $a_* = 1$ curve in Fig. 9 is very close to $g(r) = 1$, indicating that the statistics of the points in Fig. 3(a) are close to Poisson.

As the diffusion is reduced (and $a_* \equiv a\sqrt{\lambda/\kappa}$ increases) the radial distribution develops a strong peak at $r = 0$. This is evident in Fig. 9(b). This $r = 0$ peak is the signature of reproductive pair correlations—if diffusion is very weak each bug remains close to its ancestors. Thus the $r = 0$ peak in Fig. 9(b) indicates the existence of family clusters in Figs. 3(c) and (d) and the width of the peak estimates the cluster radius.

The radial distribution function of the simulations with $a_* = 16$ and 64 in Fig. 9 has an oscillatory structure. The first deep minimum of $g(r)$ indicates the “excluded area”

surrounding each isolated family in the lower panels of Fig. 3. The first maximum at nonzero r indicates the nearest-neighbour families in the first “coordination shell”. These push the next nearest neighbours into the second shell, and so on. Thus there is a sequence of oscillations with a wavelength related to the range of the competition kernel.

4. Evolution of the distribution functions: the master equation

Now we use standard arguments (e.g., Feller, 1968; van Kampen, 1997; Renshaw, 1991) to construct the exact equations determining the continuous-time evolution of the unreduced probabilities $F_k(\mathbf{X}_k, t)$ introduced back in (16). The basic idea is to model the evolution of the Brownian bug population as a one-step Markov process in continuous space and time. It helps to think of probability as flowing through the Fock space. For example, probability collects in the state $k = 0$ when a death occurs in any configuration with just one bug at any location \mathbf{x}_1 . Thus the probability of extinction, $F_0(t)$, evolves according to

$$\partial_t F_0 = \mu \int F_1(\mathbf{x}_1, t) d\mathbf{x}_1, \quad (31)$$

where μ is the death rate of the lonely bug at \mathbf{x}_1 . The next equation in the master equation formulation is the evolution of $F_1(\mathbf{x}_1, t)$:

$$[\partial_t - \kappa \nabla_1^2] F_1 = -(\mu + \lambda) F_1 + 2 \int (\mu + \nu_{12}) F_2 d\mathbf{x}_2. \quad (32)$$

On the left-hand side, diffusion acting on the single bug at \mathbf{x}_1 is represented in the usual way; ∇_1 is the gradient operator associated with \mathbf{x}_1 . Denoting the birth rate by λ , the first term on the right-hand side of (32) is the loss of $k = 1$ configurations due to either the reproduction (λ) or death (μ) of the single bug.

The second term on the right-hand side of (32), involving the integral over \mathbf{x}_2 , is the flux of probability into configurations with one bug ($k = 1$) by death in configurations with two bugs ($k = 2$). Following Bolker and Pacala (1997) we model density-dependent mortality using the competition kernel $v(r)$ introduced in (3); we use the shorthand

$$\nu_{pq} \equiv v(r_{pq}) = v(|\mathbf{x}_p - \mathbf{x}_q|). \quad (33)$$

The factor of 2 in front of the integral in (32) accounts for the possibility that either of the bugs in a $k = 2$ configuration might die.

At $k = 2$ we have for the evolution of $F_2(\mathbf{x}_1, \mathbf{x}_2, t)$

$$[\partial_t - \kappa(\nabla_1^2 + \nabla_2^2)] F_2 = \lambda F_1 \delta_{12} - 2(\mu + \nu_{12} + \lambda) F_2 + 3 \int [\mu + \nu_{13} + \nu_{23}] F_3 d\mathbf{x}_3. \quad (34)$$

The first term on the right-hand side, $\lambda F_1 \delta_{12}$, is the production of configurations with two bugs ($k = 2$) by birth in configurations with one bug ($k = 1$). Here we are

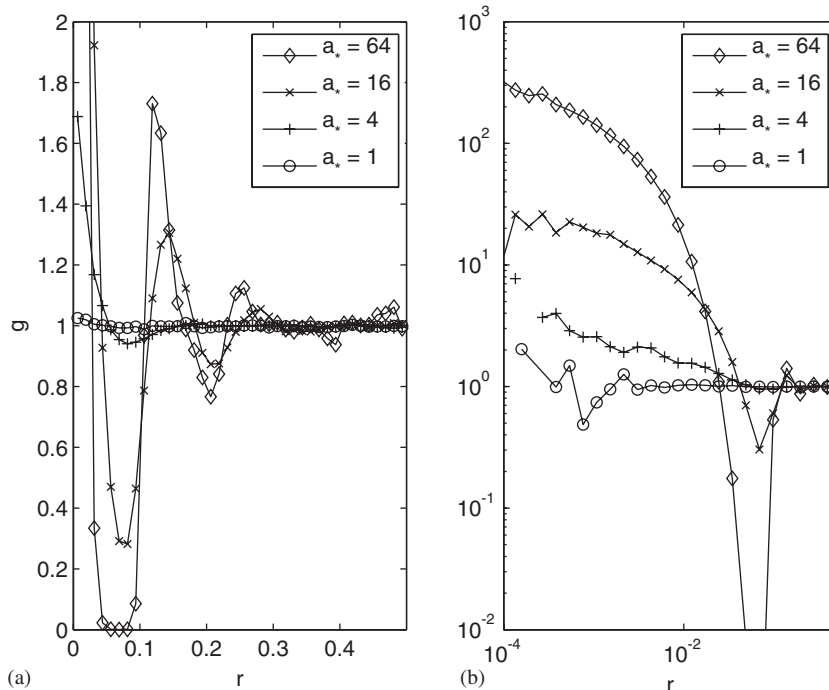


Fig. 9. Estimates of the radial distribution function, $g(r, t)$, obtained from the simulations in Fig. 3. After calculating and binning the separations of all pairs of bug we use equation (30) to estimate $g(r)$. The smooth curves above are the average of nine realizations each. The log-log plot in panel (b) resolves the large peak at very small r .

using the notation

$$\delta_{pq} \equiv \delta(\mathbf{x}_p - \mathbf{x}_q) \quad (\text{not the Kronecker-}\delta). \quad (35)$$

The δ -function ensures that the new bug is introduced at its mother's location.

The second term on the right-hand side of (34) is the flux of probability out of $k = 2$ configurations driven by births at rate 2λ and deaths at rate $2(\mu + v_{12})$. The final term on the right-hand side of (34) is the production of $k = 2$ configurations by a death in $k = 3$ configurations. The factor $v_{13} + v_{23}$ accounts for the enhanced mortality of bug 3 due to competition with the other two bugs in the configuration. The factor of 3 outside the final integral in (34) accounts for the possibility that any of the three bugs might die in dt . We turn now to the general case.

4.1. Birth and death

Suppose that a birth occurs in a configuration with $k - 1$ bugs. The rate of this process is $(k - 1)\lambda$ and therefore the ensuing loss of probability from configurations with $k - 1$ bugs is

$$\partial_t F_{k-1} + \dots = -\lambda(k - 1)F_{k-1} + \dots \quad (36)$$

The corresponding gain of probability in configurations with k bugs is

$$\partial_t F_k + \dots = +\lambda(k - 1)\mathbb{B}F_{k-1} + \dots \quad (37)$$

Above, \mathbb{B} , is a ‘‘birth operator’’ that increases the number of \mathbf{x} 's from $k - 1$ to k by introducing all $k(k - 1)/2$ of the

δ_{pq} 's, while maintaining normalization and permutation symmetry. For instance, $\mathbb{B}F_1 = \delta_{12}F_1$, and

$$\mathbb{B}F_2 = \frac{1}{3}[\delta_{12}F_2(\mathbf{x}_2, \mathbf{x}_3) + \delta_{13}F_2(\mathbf{x}_2, \mathbf{x}_3) + \delta_{23}F_2(\mathbf{x}_1, \mathbf{x}_3)]. \quad (38)$$

Writing the general expression for \mathbb{B} requires some notational elaboration. We define

$$\mathbf{X}_{k|p} = \mathbf{X}_k \quad \text{with } \mathbf{x}_p \text{ deleted.} \quad (39)$$

For example, $\mathbf{X}_{4|2} = [\mathbf{x}_1, \mathbf{x}_3, \mathbf{x}_4]$ and $\mathbf{X}_{2|1} = \mathbf{x}_2$. Using this notation, the birth operator \mathbb{B} is

$$\mathbb{B}F_{k-1} \equiv \frac{2}{k(k-1)} \sum_{1 \leq p < q \leq k} \delta_{pq} F_{k-1}(\mathbf{X}_{k|p}, t). \quad (40)$$

Notice there are $k(k - 1)/2$ terms in the double sum above. The normalization factor $2/k(k - 1)$ in (40) ensures that

$$\int \mathbb{B}F_{k-1} d\mathbf{X}_k = \int F_{k-1} d\mathbf{X}_{k-1}, \quad (41)$$

and thus probability is conserved.

Because of death, probability leaves configurations with k bugs at a rate

$$\partial_t F_k + \dots = -\left(\mu k + 2 \sum_{1 \leq p < q \leq k} v_{pq}\right) F_k + \dots \quad (42)$$

The bracketed factor on the right-hand side is the total death rate in a configuration with k bugs. The probability leaving configurations with k bugs due to a death flows into configurations with $k - 1$ bugs. This source in the

evolution equation for F_{k-1} is constructed by reducing the number of \mathbf{x} 's in F_k from k to $k-1$ via integration over \mathbf{x}_k . This reduction must conserve probability and the permutation symmetry so that

$$\partial_t F_{k-1} + \dots = +k \int \left(\mu + \sum_{p=1}^{k-1} v_{pk} \right) F_k d\mathbf{x}_k + \dots \quad (43)$$

The bracketed term inside the integral is probability per unit time that the bug at \mathbf{x}_k dies; the factor k outside the integral accounts for the possibility that any of the k bugs might die.

4.2. Summary: the master equation

Assembling the results above, the final evolution equation for $F_k(\mathbf{X}_k, t)$ with $k \geq 1$ is

$$\begin{aligned} & [\partial_t - \kappa \Delta] F_k \\ &= \lambda(k-1) \mathbb{B} F_{k-1} - \left[k(\mu + \lambda) + 2 \sum_{1 \leq p < q \leq k} \sum v_{pq} \right] F_k \\ &+ (k+1) \int \left(\mu + \sum_{p=1}^k v_{p,k+1} \right) F_{k+1} d\mathbf{x}_{k+1}. \end{aligned} \quad (44)$$

The birth operator \mathbb{B} is defined in (40) and the $k=0$ equation is given in (31). On the left-hand side of (44),

$$\Delta \equiv \sum_{p=1}^{\infty} \nabla_p \cdot \nabla_p \quad (45)$$

is the total Laplacian. Because $F_k(\mathbf{X}_k)$ does not depend on $\mathbf{x}_{k+1}, \mathbf{x}_{k+2}, \dots$, the operator Δ collapses to a finite number of terms when it acts on any F_k .

5. Reduced distribution functions: the closure problem

The reduced distribution functions or spatial moments defined in (29) summarize the most basic statistics of the population. Using definition (23) we obtain the equation for the first reduced distribution function, $f^{(1)}(\mathbf{x}_1, t)$ (the concentration), by summing and integrating the master equation (44). The $f^{(1)}$ equation is (5) with different notation:

$$(\partial_t - \kappa \Delta) f^{(1)} = \gamma f^{(1)} - \int v(\mathbf{x} - \mathbf{y}) f^{(2)}(\mathbf{x}, \mathbf{y}, t) d\mathbf{y}. \quad (46)$$

Above $\gamma \equiv \lambda - \mu$ denotes a net growth rate. Because of the density dependence, $v(r)$, the pair function, $f^{(2)}$, appears in (46) as a convolution.

To obtain the equation for the pair function, $f^{(2)}(\mathbf{x}_1, \mathbf{x}_2, t)$, we again sum and integrate the master equation (44) using the definition of $f^{(2)}$ in (28). The calculation is very similar to that for $f^{(1)}$ and the result is

$$(\partial_t - \kappa \Delta) f^{(2)} = 2\lambda \delta_{12} f^{(1)} + 2(\gamma - v_{12}) f^{(2)} - (v_{13} + v_{23}) \star f^{(3)}. \quad (47)$$

In (47) the convolutions, now denoted by \star , are integrals over \mathbf{x}_3 . The term involving $\delta_{12} = \delta(\mathbf{x}_1 - \mathbf{x}_2)$ is the source of reproductive pair correlations. For good measure, we also give the triplet equation

$$\begin{aligned} & (\partial_t - \kappa \Delta) f^{(3)} \\ &= 2\lambda(\delta_{12} f^{(2)}(\mathbf{x}_2, \mathbf{x}_3) + \delta_{13} f^{(2)}(\mathbf{x}_2, \mathbf{x}_3) + \delta_{23} f^{(2)}(\mathbf{x}_1, \mathbf{x}_3)) \\ &+ (3\gamma - 2(v_{12} + v_{13} + v_{23})) f^{(3)} \\ &- (v_{14} + v_{24} + v_{34}) \star f^{(4)}. \end{aligned} \quad (48)$$

The last term on the right-hand side of the $f^{(2)}$ equation contains $f^{(3)}$, and $f^{(4)}$ appears in the $f^{(3)}$ equation with the convolution indicating integration over \mathbf{x}_4 . In general, if $v(r) \neq 0$, the equation for each reduced distribution function contains the reduced function of the next higher order. In order to make practical use of these equations it is necessary to truncate the hierarchy (see BDLMP). Indeed, just as the master equation (44) is analogous to the Liouville equation of statistical mechanics, the spatial moment hierarchy of BDLMP above is analogous to the BBGKY hierarchy of statistical mechanics.

We note that the closure problem of the spatial correlation functions and the development of patchiness due to reproductive pair correlations are independent issues. The closure problem is due solely to pair interactions, e.g., the term involving $v(|\mathbf{x} - \mathbf{y}|)$ in (5). With $v(r) = 0$ there is no closure problem and (9) is an exact (but inadequate) ADR description of the spatial structure of the population in Fig. 1 and $G(\mathbf{x}, \mathbf{y}, t)$ can also be found exactly in this case.

6. Exact equilibrium solution of the master equation with infinite-range competition

In this section we discuss the case of infinite-range competition. This means that the competition kernel is a constant

$$v(r) = v_0, \quad (49)$$

and that the pairwise interaction does not decay with separation. With a constant competition kernel the interaction between bugs is global: every bug ‘‘feels’’ every other bug, no matter how distant. In this infinite-range case one can directly extract information from the master equation, without descent to the moment hierarchy and closure assumptions. Before turning to these analytic considerations, a simulation of the global competition model is shown in Fig. 10. The initial condition is the Poisson distribution of bugs shown in panel (a). Eventually the system reaches equilibrium with the bugs in a single clump, as in panel (b). This patch is the family of descendants from a single ur-bug, which has eliminated all other families from the domain. Thus, despite the simplicity of the infinite-range competition kernel, the spatial distribution of the equilibrium population is non-trivial.

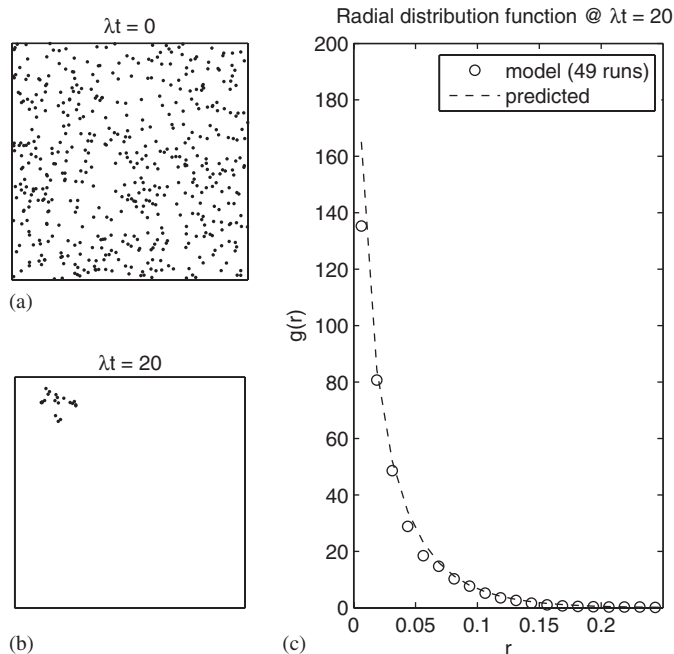


Fig. 10. The global competition model with $a/L = 1$, $\lambda/v_0 = 20$, $\mu/\lambda = 0$, $\kappa = 10^{-4}$. By $\lambda t = 20$ only a single family is extant. The radial distribution function in panel (c) has been averaged over 49 realizations for smoothness; the dashed curve is the $d = 2$ solution in (73).

6.1. The probability of k bugs with global competition

The global competition case is soluble because the distribution of the bugs in space has no effect on the population dynamics. Specifically, consider

$$p_k(t) \equiv \int F_k(t) d\mathbf{X}_k, \quad (50)$$

= probability of k bugs at time t .

With infinite-range competition, and $\mu = 0$, integration of the master equation (44) over all space yields a set of differential equations for the $p_k(t)$'s:

$$\begin{aligned} \dot{p}_1 &= -\lambda p_1 + 2v_0 p_2, \\ \dot{p}_2 &= \lambda p_1 - (2\lambda + 2v_0)p_2 + 6v_0 p_3, \end{aligned} \quad (51)$$

and in general

$$\dot{p}_k = \lambda(k-1)p_{k-1} - [k\lambda + k(k-1)v_0]p_k + v_0 k(k+1)p_{k+1}. \quad (52)$$

This is a simplified version of the logistic process in Kendall (1949) whose equilibrium solution is given in Renshaw (1991):

$$p_k = \frac{1}{k!} \left(\frac{\lambda}{v_0}\right)^k \frac{1}{\exp(\lambda/v_0) - 1}. \quad (53)$$

It is easy to check (53) by substitution into (52). We have also confirmed that the statistics of the fluctuating population in the simulation of Fig. 10 conforms to the equilibrium probability distribution in (53). Of course this

solution for p_k gives us no information about the spatial structure of the cluster in panel (b) of Fig. 10.

6.2. The spatial structure of the population with global competition

The solution of the global competition model without integration over space now proceeds as follows: With $\mu = 0$ we see from (31) that F_0 is constant. In other words, if $\mu = 0$ then $k = 1$ configurations can never transition to $k = 0$. Thus we now take $F_0 = 0$ and begin by writing (44) in the form

$$\partial_t F_k = R_k + S_k, \quad (54)$$

where

$$R_k \equiv (k-1)\lambda \mathbb{B} F_{k-1} - k(k-1)v_0 F_k + \kappa \Delta F_k, \quad (55)$$

and

$$S_k \equiv k(k+1)v_0 \int F_{k+1} d\mathbf{x}_{k+1} - k\lambda F_k. \quad (56)$$

Notice that we have used the infinite-range assumption to pull v_0 outside the \mathbf{x}_{k+1} -integral above. We solve the steady system ($\partial_t F_k = 0$) by demanding that R_k and S_k separately vanish (detailed balance). To appreciate how this procedure works, and to reach an inductive proof, we write out the first few terms explicitly. At $k = 1$ we have

$$\begin{aligned} R_1 &\equiv \kappa \Delta F_1, \\ S_1 &\equiv 2v_0 \int F_2 d\mathbf{x}_2 - \lambda F_1. \end{aligned} \quad (57)$$

At $k = 2$,

$$\begin{aligned} R_2 &\equiv \lambda \delta_{12} F_1 - 2v_0 F_2 + \kappa \Delta F_2, \\ S_2 &\equiv 6v_0 \int F_3 d\mathbf{x}_3 - 2\lambda F_2, \end{aligned} \quad (58)$$

and, for good measure, at $k = 3$,

$$\begin{aligned} R_3 &\equiv \frac{2}{3} \lambda [\delta_{12} F_2(\mathbf{x}_2, \mathbf{x}_3) + \delta_{13} F_2(\mathbf{x}_2, \mathbf{x}_3) + \delta_{2,3} F_2(\mathbf{x}_1, \mathbf{x}_3)] \\ &\quad - 6v_0 F_3 + \kappa \Delta F_3, \\ S_3 &\equiv 12v_0 \int F_4 d\mathbf{x}_4 - 3\lambda F_3. \end{aligned} \quad (59)$$

The homogeneous and isotropic equilibrium solution is now found with the ansatz

$$F_k(\mathbf{X}_k) = \frac{1}{k!} \left(\frac{\lambda}{v_0}\right)^k \frac{\mathcal{F}_k(\mathbf{X}_k)}{e^{\lambda/v_0} - 1}. \quad (60)$$

For (60) to satisfy the normalization condition (17) we require

$$\int \mathcal{F}_k(\mathbf{X}_k) d\mathbf{X}_k = 1. \quad (61)$$

The guess in (60) and (61) is motivated by the form of the spatially integrated solution in (53).

Starting with $k = 1$, to make the ansatz (60) satisfy (57) and (61) we take

$$\mathcal{F}_1 = \Omega^{-1} \quad \text{and} \quad \int \mathcal{F}_2(r) \, d\mathbf{r} = \mathcal{F}_1, \quad (62)$$

where Ω is the area of the domain. Turning to $k = 2$, substituting the ansatz (60) into (58), and demanding that $R_2 = 0$, give

$$\ell^2 \Delta \mathcal{F}_2 - 2\mathcal{F}_2 + 2\mathcal{F}_1 \delta(\mathbf{r}) = 0, \quad (63)$$

where

$$\ell^2 \equiv \kappa/v_0. \quad (64)$$

Above $\mathbf{r} \equiv \mathbf{x}_2 - \mathbf{x}_1$, and because of isotropy and homogeneity \mathcal{F}_2 is a function only of $r \equiv |\mathbf{r}|$ so that $\Delta \mathcal{F}_2 = 2\nabla_r^2 \mathcal{F}_2$. Integrating (63) over $d\mathbf{r}$ we now see that the integral constraint on \mathcal{F}_2 in (62) is satisfied—this is the first indication of how the ansatz works. But demanding that $S_2 = 0$ in (58) now gives another integral constraint

$$\int \mathcal{F}_3 \, d\mathbf{x}_3 = \mathcal{F}_2. \quad (65)$$

Now at $k = 3$, substituting the ansatz (60) into (59) gives

$$\ell^2 \Delta \mathcal{F}_3 - 6\mathcal{F}_3 + 2[\delta_{12} \mathcal{F}_2(r_{23}) + \delta_{13} \mathcal{F}_2(r_{23}) + \delta_{23} \mathcal{F}_2(r_{13})] = 0, \quad (66)$$

and also

$$\int \mathcal{F}_4 \, d\mathbf{x}_4 = \mathcal{F}_3. \quad (67)$$

Integrating (66) over \mathbf{x}_3 and using (63) show that \mathcal{F}_3 indeed satisfies the integral constraint in (65).

The considerations above work at every order. Demanding that $S_k = 0$ gives the integral constraint

$$\int \mathcal{F}_{k+1} \, d\mathbf{x}_{k+1} = \mathcal{F}_k. \quad (68)$$

The condition $R_k = 0$ determines \mathcal{F}_k as the solution of

$$\ell^2 \Delta \mathcal{F}_k - k(k-1)\mathcal{F}_k + k(k-1)\mathbb{B}\mathcal{F}_{k-1} = 0. \quad (69)$$

Integrating the equation above over $d\mathbf{x}_k$ verifies that \mathcal{F}_k satisfies the integral constraint obtained at the previous order, $k-1$. The essential intermediate identity used in this inductive proof is

$$(k+1) \int \mathbb{B}F_k \, d\mathbf{x}_{k+1} = 2F_k + (k-1)\mathbb{B} \int F_k \, d\mathbf{x}_k, \quad (70)$$

where \mathbb{B} is the birth operator defined in (40).

This looks like a pyrrhic victory because it is increasingly difficult to solve (69) as k increases. However, if we are content with the reduced distribution functions $f^{(1)}$ and $f^{(2)}$ then we can make progress. The key is that the integral constraint (68) greatly simplifies the definition of $f^{(s)}(\mathbf{X}_s)$. Specifically, one finds that

$$f^{(s)}(\mathbf{X}_s) = \frac{(\lambda/v_0)^s}{1 - e^{-\lambda/v_0}} \mathcal{F}_s(\mathbf{X}_s). \quad (71)$$

Thus, remarkably, F_k and $f^{(k)}$ are proportional to the function \mathcal{F}_k defined by (69). Explicitly then, using (62) and (71), the equilibrium concentration with infinite-range competition is

$$f^{(1)} = \frac{\lambda/v_0}{1 - e^{-\lambda/v_0}} \frac{1}{\Omega}. \quad (72)$$

To obtain the pair function we assume that $\ell \ll \Omega^{1/d}$ and solve (63). Using (71) the result is

$$f^{(2)} = \frac{(\lambda/v_0)^2}{1 - e^{-\lambda/v_0}} \frac{1}{\Omega \ell^2} \times \begin{cases} (\ell/2) \exp(-|\bar{r}|), & d = 1; \\ (2\pi)^{-1} K_0(|\bar{r}|), & d = 2; \\ (4\pi r)^{-1} \exp(-|\bar{r}|), & d = 3. \end{cases} \quad (73)$$

Above, $\bar{r} \equiv r/\ell$.

7. Weak diffusion, and the form of the competition kernel

The infinite-range competition of Section 6 seems contrived. But this special case helps explain the result from Section 2 that the total population can increase in response to decreasing diffusion. In particular, notice that the non-dimensional parameter $a_* \equiv a\sqrt{\lambda/\kappa}$ is increased by either reducing diffusion, κ , or increasing the range, a . To illustrate this correspondence, Fig. 11 shows a simulation with $a/L = \frac{1}{10}$ with no diffusion (that is, $a_* = \infty$). In this case bugs cannot move away from their parents, and so

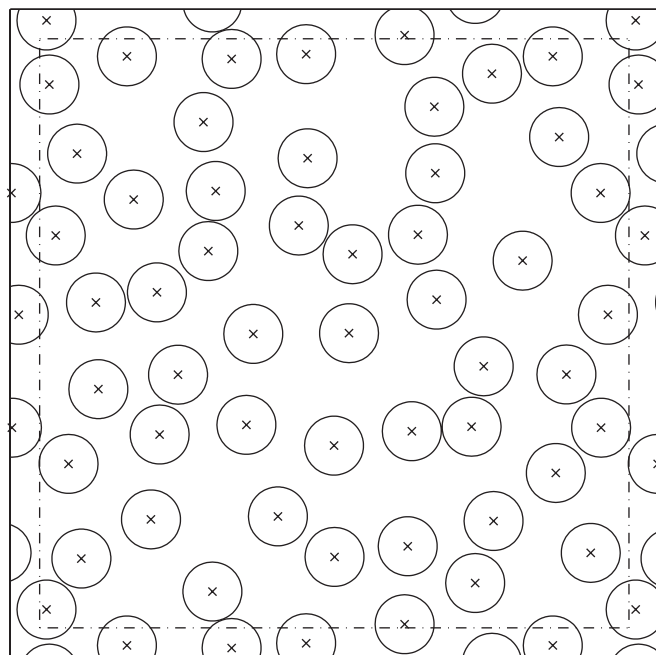


Fig. 11. The non-diffusive case in $d = 2$ at $\lambda t = 100$. Only 50 of the original 2000 families have survived. The total population $N \approx 1.7 \times N_0$, where N_0 is the population predicted by the SLE in (13). The locations of the surviving families are indicated by the \times symbol and the circles have radius $a/2$. Overlap between circles would indicate competition between surviving families. The parameters for this simulation are $\lambda t = 100$, $a/L = \frac{1}{10}$, $\lambda/v_0 = 20$, $\lambda/\mu = \infty$, $a_* = \infty$.

each surviving family occupies a single point marked with the symbol \times . The circles in Fig. 11 have radius $a/2$ (not $a!$). If any of the circles overlapped then the families they contain would be competing. However, none of the circles overlap in Fig. 11, and therefore each surviving family in the non-diffusive case effectively acts as an independent realization of the global competition case in Fig. 10. Thus, with no diffusion, the system spontaneously forms a pattern that eliminates competition between surviving families, and the size of each family follows exactly the same statistics as an ensemble with global competition, namely p_k in (53). The result of this pattern is the elevated population in Fig. 11, where $N = 1.7N_0$. We emphasize that the simulation in Fig. 11 is obtained with no diffusion. However we expect the case of weak diffusion, that is, $a_* \gg 1$, to behave similarly.

7.1. Optimal packing with the top-hat kernel

The counterintuitive result that the population increases as diffusion decreases (see Fig. 4) may be rationalized by considering the case of no diffusion and deliberately packing as many families into the plane as possible by minimizing inter-family competition. The solution is to place the families on a triangular lattice with edge length a , the competition radius, so that then there is no inter-family competition. This arrangement results in each family occupying a hexagonal territory with apothem $a/2$ and area $a^2\sqrt{3}/2$. Using (53) to obtain the expected population of a single family, the expected aggregate population is then

$$N = \frac{2L^2 \lambda}{\sqrt{3}a^2 v_0} \frac{1}{1 - e^{-\lambda/v_0}}. \tag{74}$$

Recall now that for the top-hat kernel the stationary solution of the SLE (1) predicts that the aggregate population is $N_0 = L^2\lambda/\pi a^2 v_0$. The ratio of the population of the hexagonally packed case in (74) to N_0 is therefore $N/N_0 = 2\pi/\sqrt{3} \approx 3.63$.³ The lesson is that by deliberately cultivating the bugs in a triangular lattice the aggregate population can be greatly increased above that of the strong-diffusion limit, N_0 .

Of course, in the simulations of Figs. 4 and 11 the families are never optimally packed, and so the ratio N/N_0 is always well below the optimal level 3.63, but N/N_0 is greater than 1. The optimal packing calculation correctly indicates how organizing the population into well-separated families might elevate the total population above that of the strong-diffusion limit, N_0 in (13). In simulations with weak diffusion the inter-family spacing is evident in the radial distribution function: the peaks of $g(r)$ are separated by a little more than a , the competition radius (see Fig. 9). The width of the big peak at the origin, $\ell = \sqrt{\kappa/v_0}$, is obtained from the solution in the previous section.

³We are interested in the regime with λ/v_0 substantially larger than one and so we are neglecting $\exp(-\lambda/v_0)$ in (74).

7.2. A family of competition kernels and the weak-diffusion limit

We showed in Section 2 that in the weak-diffusion limit the aggregate population is sensitive to the form of the competition kernel. This sensitivity is strikingly illustrated by comparing the top-hat result in Fig. 11 to zero-diffusion simulations using the Gaussian competition kernel in (14). With a Gaussian kernel there is an unavoidable interaction even with distant neighbors. Consequently, one finds with a Gaussian kernel that at very long times there is a single surviving family.⁴ With the Gaussian kernel, organization into a non-competitive pattern is impossible.

To explore the transition between the Gaussian and top-hat cases more fully we now consider a family of competition kernels, $v(r, m)$, with a parameter m controlling the shape of the kernel: $m = 0$ is the top-hat kernel and $m = \infty$ is the Gaussian kernel. Specifically, we propose the following family of competition kernels:

$$v(r, m) = \begin{cases} \frac{(m+1)\eta}{\pi R_m^2} \left[1 - \left(\frac{r}{R_m} \right)^2 \right]^m & \text{if } r \leq R_m, \\ 0 & \text{if } r \geq R_m. \end{cases} \tag{75}$$

The range, R_m , in (75) is defined by

$$R_m = a\sqrt{1 + \frac{1}{2}m}, \tag{76}$$

where a is the “integral length”. This definition ensures that the kernel is normalized for all m ,

$$\eta = \int v(r, m) dx, \tag{77}$$

and that the squared “radius of gyration”,

$$\int r^2 v(r, m) dx \Big/ \int v(r, m) dx, \tag{78}$$

is equal to $a^2/2$. Thus the integral length a grossly characterizes the distance over which $v(r, m)$ falls from its central maximum to a substantially smaller value. By analogy with Section 2, we measure the strength of diffusion relative to the integral scale a using the non-dimensional parameter $a_* \equiv a\sqrt{\lambda/\kappa}$. Note that if m is large, so that $v(r, m)$ approaches a Gaussian, then the range R_m is much larger than the integral length a .

Fig. 12(a) shows $v(r, m)$ deforming smoothly from a top-hat to a Gaussian as m increases from zero to infinity. To probe the effect of the competition-kernel shape on the average population we fix a_* , a/L , λ and η and vary only the shape parameter m . The SLE then predicts that the total population is $N_0 = \lambda L^2/\eta$. Fig. 12(b) shows the average populations obtained from simulations using

⁴If $v \sim \exp(-r^2/a^2)$ then the final two surviving families compete with a weak interaction, proportional to $\exp(-S^2/2\ell^2)$, where S is separation of the families which is comparable to the system size L . Thus with Gaussian interaction one family drives the other to extinction over a time which diverges like roughly $\exp(+L^2/2\ell^2)$.

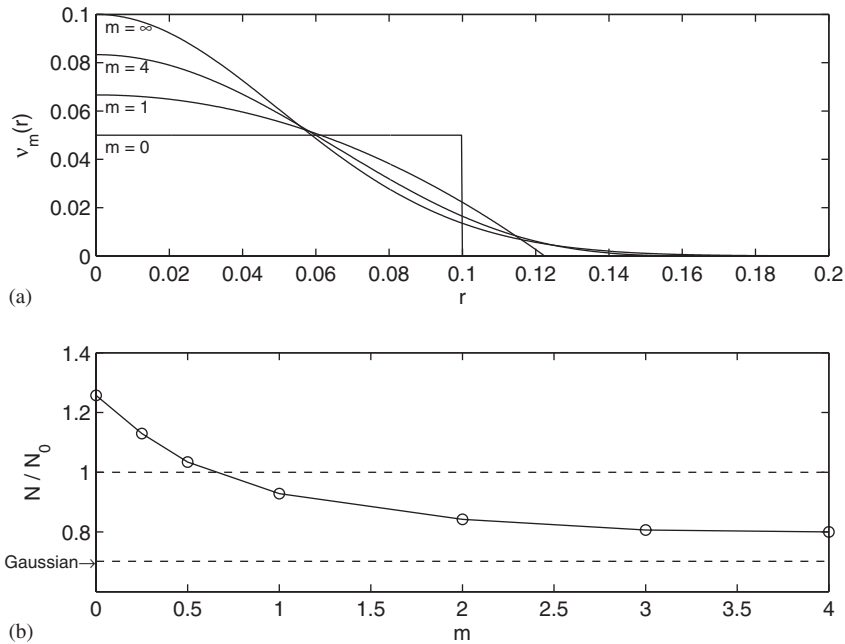


Fig. 12. (a) The kernel in (75) as a function of r for various values of m . The Gaussian limit is $v(r, \infty) = 2\eta \exp(-2r^2/a^2)/\pi a^2$. (b) The steady-state population as a function of m . In these simulations $a/L = 10$, $a_* = 20$, $\mu = 0$ and $\lambda\pi a^2 = 20\eta$.

different values of m . In the cases of $m = 0, 1/4, 1/2$ the average population exceeds the SLE prediction N_0 . However, as m increases and the kernel widens, the population falls below $N_0 = \lambda L^2/\eta$. Thus we pass smoothly between the top-hat and Gaussian limits by varying only the shape parameter m . There are significant changes in the total population during this transition.

We can rationalize the result in Fig. 12(b) by repeating the optimal packing calculation (74) using the kernel in (75). To completely eliminate inter-family competition the families are separated by the range R_m in (76) instead of a . But the intrafamily competition is given by $v(0, m)$. We find that in the optimal configuration the generalization of (74) is

$$N = \frac{2\pi\lambda L^2}{\sqrt{3}(m+1)\eta} \frac{1}{1 - e^{-\lambda/v_0}}. \quad (79)$$

Taking the Gaussian limit ($m \rightarrow \infty$), with fixed system size L , we see that the total population vanishes with optimal packing. It is amusing that if $m \leq m_c$, where

$$m_c = \frac{2\pi}{\sqrt{3}} - 1 \approx 2.63, \quad (80)$$

then the optimal value in (79) is greater than $N_0 = \lambda L^2/\eta$.⁵ In other words, if $m \leq m_c$ then farming is more productive than rapid dispersion.

⁵The populations in Fig. 12(b) drop below N_0 for $m \approx 0.6 < m_c$. This indicates that these simulations are far from optimal packing.

8. Conclusions and discussion

We have derived the master equation (44) for an individual-based model with constant reproductive rate and a death rate depending only on pairwise interactions. The master equation is exact, but also complicated and intractable. However, from the master equation one can derive the exact equations for the reduced distribution functions, for example (46)–(48), and so make contact with earlier work based on this open hierarchy of moments (BDLMP). With non-zero $v(r)$ the equations for the reduced distribution functions form an open hierarchy. One must seek closure via approximation, the simplest being the Poisson assumption (6). The Poisson assumption yields the familiar spatial logistic equation (1). Through simulation we have shown that the predictions of the SLE are a valid approximation of the underlying individual-based model only if diffusion is strong in the sense that a_* is small. If the diffusion is weak then the total population predicted by the SLE can be too high or too low depending on the parameters (Fig. 4) and the form of the competition kernel (Fig. 12). The spatial logistic equation totally misses the percolation transition and predicts populations that are much too high for non-percolating parameter values. All these failures of the SLE are due to the strong reproductive correlations which void the Poisson assumption (6) unless $a_* \ll 1$.

We have discussed two special complementary cases in which exact analytic results are possible. First, in the non-interacting case, $v = 0$, the hierarchy of reduced distribution functions closes without approximation. Felsenstein (1975) obtained the pair function in this case, and it is easy

to repeat his calculation by solving (47) with $v = 0$. This is the very simplest model describing patchiness and cluster formation. As such, the case $v = 0$ is important because reproductive pair correlations continue to operate even with nonzero v . The second case in which exact analytic results are possible is the infinite-range interaction model of Section 6. This solution is useful in understanding the case of very weak diffusion (e.g., as in Fig. 11). In this second case the BDLMP hierarchy is unclosed and so this analytic solution provides the only example of exact closure known to us.

For the case of weak diffusion, $a_* \ll 1$, the shape of the competition kernel becomes important. The optimal packing calculation (74) helps us understand this irksome sensitivity to seemingly unimportant details of the competition kernel, such as the weak exponential tail of the Gaussian. For compact kernels like the top-hat—or small m in (75)—the average population is greater than the SLE prediction. However, for diffuse kernels such as the Gaussian—or large m in (75)—the average population is always less than the SLE prediction (Fig. 12). Both these results are consistent with calculations based on maximizing the population by arranging non-interacting families of bugs on a hexagonal lattice.

A point of discussion in previous papers (Hernández-García and López, 2004; Shnerb, 2004) has been the cause of clusters such as those in Figs. 1, 3, and 13. Invoking the non-local version of the SLE mentioned after (8), these authors attribute the clusters to an instability of the homogeneous state which is controlled by the Fourier transform of the competition kernel. This non-local SLE

theory predicts that a spatially uniform population is a stable solution with the Gaussian kernel, but is unstable with the top-hat kernel. However, the Gaussian simulation in Fig. 13(c) and (d) is strongly clustered. Thus the nonlocal SLE proves unreliable in the weak-diffusion limit. The main difference between the two radial density functions in Fig. 13 is depth of the first minimum and the strength of the successive oscillations. These features are stronger in the top-hat case in Fig. 13(b), indicating greater long-range spatial order in the positions of the clusters. But contrary to the predictions of the nonlocal SLE, spontaneous cluster generation is a robust feature of *both* Gaussian and top-hat kernels.

To avoid the curious behavior of the top-hat kernel and the infinite-range interactions of the Gaussian kernel one might prefer a kernel that is both compact and smooth, such as $m = 2$ in (75). This ensures that families separated by a distance greater than the range cannot drive each other to extinction. Obviously, the value of m could vary between species and a density-dependent death rate may not be the ideal mechanism for modeling interactions between organisms. However, the main point is that the precise shape of the competition kernel can have a dramatic effect on the outcome of models and one can plausibly speculate that in the weak diffusion limit this extends to other forms of interactions.

We conclude by mentioning one aspect of the model which, with hindsight, we regard as unfortunate, or at least special. We have followed BDLMP and made the death rate depend on the local density using the competition kernel. An alternative model assumption is to make the birth rate depend on the local density through a similar construction (e.g., Hernández-García and López, 2004, 2005; Bolker and Pacala, 1999). At the crude level of the SLE there is no difference between these model strategies: they both produce a quadratic saturation term. However, it is likely that the resulting individual-based models have different properties in the low-diffusion limit. We believe that in many situations density-dependent birth is likely to be a better model of intra-specific competition than density-dependent mortality.

Acknowledgements

We thank Neil Balmforth, Charlie Doering, Mark Ohman, Nadav Shnerb, Richard Law and Adrian Martin for discussions related to this paper. We also thank two anonymous reviewers and the editor, Benjamin Bolker, for helpful comments. We gratefully acknowledge the support of the National Science Foundation through Grant OCE 0220362.

Appendix A

The Brownian bug model can be simulated on a computer as follows: First, prepare the initial condition ($t = 0$) by randomly and independently placing $k_0 \gg 1$

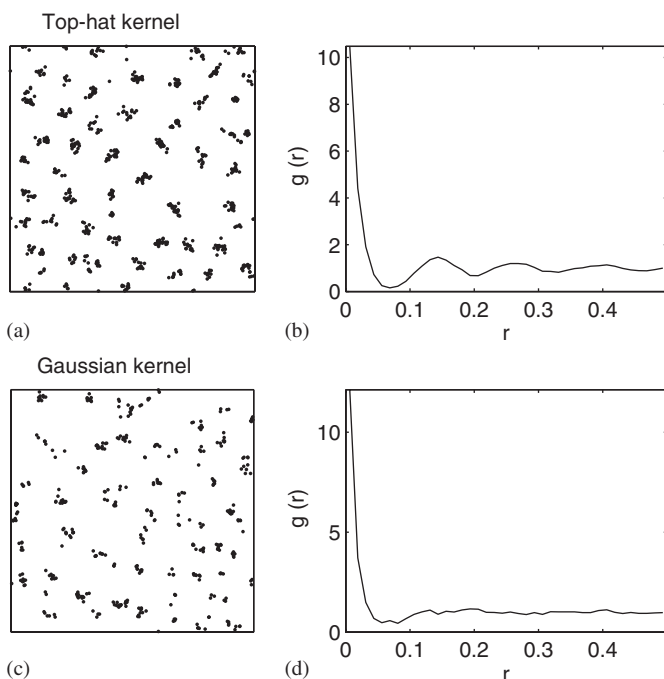


Fig. 13. (a) 797 bugs at $\lambda t = 2000$, with a top-hat kernel $a_* = 20$. (b) The radial distribution function for (a). (c) 433 bugs at $\lambda t = 2000$, with a Gaussian kernel and $a_* = 20$. (d) The radial distribution function for (c).

Brownian bugs (idealized as points) in the $L \times L$ square domain. For simplicity we consider the domain to be periodic.

Second, repeat the following sequence of steps until the desired simulation time has elapsed: determine the time to the next event (birth or death), determine the type of event, determine which bug performs the event, execute the event, and diffuse all bugs.

The simulation is event-driven and advanced through time using exponentially distributed inter-event times in the manner described by Renshaw (1991). The time to the next event, τ , is equal to $-\ln(Y)/R$ where Y is a uniformly distributed random number on $(0, 1)$ and R is the total rate of events (births and deaths). If the population is k bugs, the total rate is $R = B + D$, where B is the birth rate:

$$B = \lambda k, \quad (81)$$

and D is the death rate:

$$D = \mu k + 2 \sum_{1 \leq p < q \leq k} v(|\mathbf{x}_p - \mathbf{x}_q|). \quad (82)$$

The calculation of the double sum in D is the most time consuming routine in the simulation and is performed using the neighbor-counting scheme in Rapaport (1995). The periodicity of the domain must be taken into account by calculating the distance between two bugs in the x -direction (and similarly in the y -direction) according to

$$|x_1 - x_2| = \text{minimum}\{\text{abs}(x_1 - x_2), L - \text{abs}(x_1 - x_2)\}. \quad (83)$$

A second uniformly distributed random number determines whether the event is a birth (with probability B/R) or a death (with probability D/R). A third random number determines which bug performs the event. If the event is a birth then each bug is equally likely to have performed the event. If the event is a death then the probability of selecting a particular bug is weighted according to the magnitude of that bug's contribution to the death rate in (82).

Finally, every bug diffuses with diffusivity, κ , which amounts to a step of normally distributed length with root mean square value $2\sqrt{\kappa\tau}$ in a random direction (uniformly distributed on $(0, 2\pi)$). Periodic boundary conditions are used to handle bugs which diffuse out of the domain.

References

Adler, R., 1997. Superprocesses and plankton dynamics. In: Monte Carlo Simulation in Oceanography. Proceedings of the 'Aha Huliko'a Hawaiian Winter Workshop, University of Hawaii at Manoa.

Bolker, B.M., Pacala, S.W., 1997. Using moment equations to understand stochastically driven spatial pattern formation in ecological systems. *Theor. Popul. Biol.* 52, 179–197.

Bolker, B.M., Pacala, S.W., 1999. Spatial moment equations for plant competition: understanding spatial strategies and the advantages of short dispersal. *Am. Nat.* 153, 575–602.

Dieckmann, U., Law, R., Metz, J.A.J., 2000. *The Geometry of Ecological Interactions: Simplifying Spatial Complexity*. Cambridge University Press, Cambridge, UK, 564 + xiv pp.

Doering, C.R., Sargsyan, K.V., Sanders, L.M., 2005. Extinction times for birth–death processes: exact results continuum asymptotics and the failure of the Fokker–Planck approximation. *SIAM J. Multiscale Modeling Simulation* 3, 283–299.

Doi, M., 1976a. Second quantization representation for classical many-particle system. *J. Phys. A* 9, 1465–1477.

Doi, M., 1976b. Stochastic theory of diffusion-controlled reaction. *J. Phys. A* 9, 1479–1495.

Etheridge, A.M., 2000. *An Introduction to Superprocesses*. University Lecture Series, vol. 20. American Mathematical Society, Providence, RI, 187 + xii pp.

Feller, W., 1968. *An Introduction to Probability Theory and its Applications*, third ed., vol. I. Wiley, New York, 509 + xviii pp.

Felsenstein, J., 1975. A pain in the torus: some difficulties with models of isolation by distance. *Am. Nat.* 109, 359–368.

Fisher, R.A., 1937. The wave of advance of advantageous genes. *Ann. Eugen.* 7, 355–369.

Fuentes, M.A., Kuperman, M.N., Kenkre, V.M., 2004. Nonlocal interaction effects on pattern formation in population dynamics. *Phys. Rev. Lett.* 91, 158104.

Hernández-García, E., López, C., 2004. Clustering, advection and patterns in a model of population dynamics with neighborhood-dependent rates. *Phys. Rev. E* 70, 016216.

Hernández-García, E., López, C., 2005. Birth, death and diffusion of interacting particles. *J. Phys.: Condens. Matter* 17, S4263–S4274.

Kendall, D.G., 1949. Stochastic processes and population growth. *J. R. Stat. Soc. Ser. B Methodological* 11, 230–282.

Kessler, D.A., Levine, H., Ridgway, D., Tsimring, L., 1997. Evolution on a smooth landscape. *J. Stat. Phys.* 87, 519–544.

Kolmogorov, A., Petrovsky, I., Piscunov, H., 1937. Study of the diffusion equation with growth of the quantity of matter and its application to a biology problem. In: Pelcé, P. (Ed.), *Originally published in Bulletin de l'Université d'état à Moscou Série Internationale, Section A, 1, 1937. For an English translation see: Dynamics of Curved Fronts, 1988. Academic Press, San Diego, 514 + xv pp.*

Law, R., Murrel, D.J., Dieckmann, U., 2003. Population growth in space and time: spatial logistic equations. *Ecology* 84, 252–262.

Martin, A.P., 2004. A Malthusian curb on spatial structure in microorganism populations. *J. Theor. Biol.* 230, 343–349.

Maruvka, Y.E., Shnerb, N.M., 2005. Nonlocal competition and logistic growth: patterns, defects and fronts. *arXiv:nlin.PS/0506046*.

Meyer, M., Havlin, S., Bunde, A., 1996. Clustering of independently diffusing individuals by birth and death process. *Phys. Rev. E* 54, 5567.

Rapaport, D.C., 1995. *The Art of Molecular Dynamics Simulation*. Cambridge University Press, Cambridge, 549 + xiii pp.

Renshaw, E., 1991. *Modelling Biological Populations in Space and Time*. Cambridge University Press, Cambridge, 403 + xvii pp.

Shnerb, N.M., 2004. Pattern formation and nonlocal logistic growth. *Phys. Rev. E* 69, 061917.

Skellam, J.G., 1951. Random dispersion in theoretical populations. *Biometrika* 38, 196–218.

Slade, G., 2002. Scaling limits and super-Brownian motion. *Not. Am. Math. Soc.* 49, 1056–1067.

van Kampen, N.G., 1997. *Stochastic Processes in Physics and Chemistry*, second ed. North-Holland, Amsterdam, 465 + xiv pp.

Young, W.R., Roberts, A.J., Stuhne, G., 2001. Reproductive pair correlations and the clustering of organisms. *Nature* 412, 328–331.

Zhang, Y.-C., Serva, M., Polikarpov, 1990. Diffusion reproduction processes. *J. Stat. Phys.* 58, 849–861.